ChemComm

COMMUNICATION

View Article Online
View Journal | View Issue

Cite this: *Chem. Commun.*, 2016, 52, 4481

Received 21st January 2016,
Accepted 25th February 2016

DOI: 10.1039/c6cc00577b

www.rsc.org/chemcomm

Flowerlike WSe_2 and WS_2 microspheres: one-pot synthesis, formation mechanism and application in heavy metal ion sequestration†

Wei Li,[a] Dehong Chen,[b] Fang Xia,[ac] Jeannie Z. Y. Tan,[ab] Jingchao Song,[ad] Wei-Guo Song[e] and Rachel A. Caruso*[ab]

Flowerlike WSe_2 and WS_2 microspheres were synthesized by a facile and scalable one-pot solvothermal method. Their formation mechanism followed the reaction between dissolved $W(CO)_6$ and dissolved S or melted Se without complete decomposition of $W(CO)_6$ into tungsten. As novel efficient sorbents, WSe_2 and WS_2 demonstrated outstanding uptake capacities for Pb^{2+} and Hg^{2+}.

Layered transition metal dichalcogenides (TMDs), MX_2 where M is a transition metal (such as Mo, W, and Nb) and X is a chalcogen (S, Se and Te), have received intensive research interest due to their unique electronic, optical, mechanical and chemical properties.[1] Among them, WSe_2 and WS_2 have been extensively studied for a variety of applications including valleytronics,[2] batteries,[3] electrocatalysis,[4] photocatalysis,[5] bioimaging labels,[6] and electronic devices.[7] WSe_2 and WS_2 have a layered structure in the form of Se–W–Se or S–W–S with a W atomic layer sandwiched by two hexagonal chalcogen atomic layers.[4a,b] The interlayers are coupled by weak van der Waals forces and the intralayer W–Se/S bonding is covalent.[1] Most reports focus on the fabrication of nanosheets/nanotubes of WSe_2 and WS_2 by chemical vapor deposition (CVD), electrochemical exfoliation and hot-injection approaches.[2–7] These methods require high temperature, expensive precursors or toxic H_2S/H_2Se, and harsh conditions that give low yields. The growth mechanisms of TMDs have been rarely described, although the formation mechanisms of similar lamellar bismuth chalcogenide materials have been explored.[1e,f] Moreover, there are few reports on the construction of three-dimensional (3D) hierarchical nanosheet-assembled flowerlike architectures of WSe_2, although 3D flowerlike MoS_2 and metal oxides or hydroxides such as FeOOH and AlOOH have been widely studied.[8] WS_2 nanoflowers were produced by using CVD with low yields.[9] Hierarchical nanosheets assembled into flowerlike structures normally show superior performance in batteries and water treatment.[8,10] Therefore, it is highly desirable to develop hierarchical WSe_2 and WS_2 using a facile, cost-effective and scalable approach.

As a new class of heavy metal ion scavenger, metal chalcogenides have been used in heavy metal ion sequestration for water treatment, including ZnS, $K_{2x}Mn_xSn_{3-x}S_6$, $(NH_4)_4In_{12}Se_{20}$, $H_{2x}Mn_xSn_{3-x}S_6$ and $H_xNa_yInS_z$,[11] due to the strong affinity of the chalcogen to heavy metal ions. In this study, flowerlike WSe_2 and WS_2 microspheres consisting of their corresponding nanosheets were synthesized by a simple, low-cost and high-yield one-pot template-free solvothermal approach. Their growth mechanism was elucidated by *in situ* synchrotron radiation X-ray diffraction (SR-XRD). WSe_2 and WS_2 were used in heavy metal ion sequestration for the first time and showed exceptional uptake capacities for Pb^{2+} and Hg^{2+}, making them ideal candidates for heavy metal remediation in practical water purification.

WSe_2 and WS_2 were prepared in high yields (>3 g) by a solvothermal method from the reaction of $W(CO)_6$ and Se or S powders in *p*-xylene (see details in ESI†). Fig. 1 shows the scanning electron microscopy (SEM) and transmission electron microscopy (TEM) images of the flowerlike WSe_2. The WSe_2 sample displays a hierarchical flowerlike micro/nanostructure (Fig. 1). The flowerlike WSe_2 is composed of many self-assembled petals that are curly nanosheets (Fig. 1c). These WSe_2 nanosheets are 5 nm in thickness and 300 nm in width, and are assembled together to form 3D WSe_2 flowers with diameters ranging from 500 nm to 1 μm. Fig. 1d demonstrates that the thin WSe_2 nanosheets consist of a few layers (<10 layers) stacking together and the interlayer spacing of the nanosheets is 0.689 nm, corresponding to the (002) plane of the hexagonal WSe_2, with slight expansion due to the strain from the layer curvature.[3b] The lattice spacing of 0.285 nm corresponds to the (100) plane of the 2H–WSe_2 phase. The X-ray diffraction

[a] *CSIRO Manufacturing, The Commonwealth Scientific and Industrial Research Organization (CSIRO), Clayton South, Victoria, 3169, Australia*
[b] *Particulate Fluids Processing Centre, School of Chemistry, The University of Melbourne, Parkville, Victoria, 3010, Australia. E-mail: rcaruso@unimelb.edu.au*
[c] *School of Engineering and Information Technology, Murdoch University, Murdoch, Western Australia, 6150, Australia*
[d] *Department of Materials Science and Engineering, Monash University, Clayton, Victoria, 3800, Australia*
[e] *Beijing National Laboratory for Molecular Sciences (BNLMS), Institute of Chemistry, Chinese Academy of Sciences, Beijing, 100190, P. R. China*
† Electronic supplementary information (ESI) available. See DOI: 10.1039/c6cc00577b

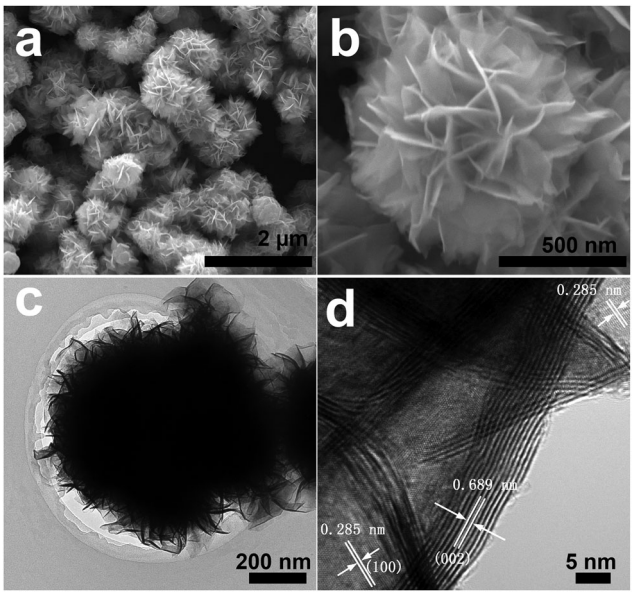

Fig. 1 SEM images (a and b) and TEM images (c and d) of the WSe_2 microspheres.

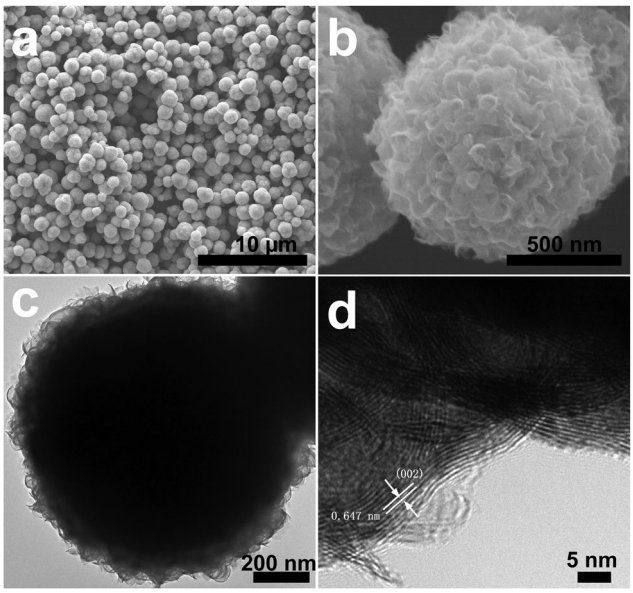

Fig. 2 SEM images (a and b) and TEM images (c and d) of the WS_2 microspheres.

(XRD) pattern (Fig. S1a, ESI†) is indexed to the hexagonal 2H–WSe_2 structure (JCPDS Card No. 38-1388). The energy dispersive X-ray (EDX) spectroscopy confirms the composition of WSe_2 with a W/Se atomic ratio of 0.51 (Fig. S1b, ESI†), in good agreement with the result (W/Se atomic ratio = 0.54) from inductively coupled plasma optical emission spectroscopy (ICP-OES). The X-ray photoelectron spectroscopy (XPS, Fig. S2, ESI†) shows that the W $4f_{7/2}$ (31.9 eV) and W $4f_{5/2}$ (34.0 eV) peaks are consistent with previous studies of WSe_2 samples.[4a,12] The small peaks at 35.6 eV and 37.8 eV are assigned to W $4f_{7/2}$ and W $4f_{5/2}$ from WO_3, likely due to oxidation because of exposure to air during sample preparation and transfer for XPS characterization, and were observed in previous WSe_2 reports.[4a,12] The Se 3d peak was located at 54.4 eV which could be deconvoluted into $3d_{5/2}$ and $3d_{3/2}$ peaks.

A similar solvothermal approach using sulfur powder instead of selenium produced a WS_2 sample. The product is composed of microspheres with an average diameter of 1 μm (Fig. 2a). The WS_2 microsphere is comprised of curly nanosheets (Fig. 2b and c), yet with smaller width (several tens of nanometers) compared to that of the WSe_2 nanosheets. The WS_2 nanosheets consist of 5–10 layers and the interlayer distance is 0.647 nm corresponding to the (002) plane of the hexagonal WS_2 (Fig. 2d). The XRD pattern (Fig. S3a, ESI†) can be assigned to the hexagonal 2H–WS_2 structure (JCPDS Card No. 84-1398), yet with a small shift in (002) peak towards low angle, which is probably caused by the layer curvature.[3b] Both the EDX spectroscopy (Fig. S3b, ESI†) and ICP-OES results show the presence of W and S in the WS_2 microspheres with a W/S atomic ratio close to 0.5. The XPS spectra (Fig. S4, ESI†) display the W $4f_{7/2}$, W $4f_{5/2}$ and W $5p_{5/2}$ peaks as well as S 2p peak consistent with previous reported WS_2 samples, corroborating that the sample is pure WS_2 without oxidation.[4b,c,5b]

These results demonstrate that the solvothermal method is efficient in producing nanosheet self-assembled 3D WSe_2 and WS_2 micro/nanostructures in high yields. The presence of nanosheets in this architecture enhances the surface-to-volume ratio and offers more accessible interfaces for sequestration, while the entire microstructure enables fast and easy sedimentation and separation from water.[8a–c]

In order to unravel the growth mechanism of flowerlike WSe_2 and WS_2 microspheres, the synthesis conditions, including temperature and reaction time, were varied and the samples were characterized by SEM and *ex situ* XRD.

For WSe_2, the optimal temperature is 250 °C, which is above the melting point (m.p.) of Se (221 °C). Below 250 °C, there was residual Se in the product (Fig. S5 & S6, ESI†). WS_2 microspheres formed at 150 °C and crystallized upon rising temperature and the morphology evolved from irregular microspheres with smooth surfaces to relatively uniform microspheres with a well-defined nanosheet assembly (Fig. S7, ESI†). At 250 °C, the smooth WSe_2 microspheres gradually developed into coarse spheres with improved crystallinity and eventually crystalline flowerlike WSe_2 formed (Fig. S8, ESI†), as the reaction time was prolonged. A similar process also occurred in the growth of WS_2 microspheres except that the lateral size of the WS_2 nanosheets was smaller than that of the WSe_2 nanosheets (Fig. S9, ESI†). Therefore, for both WSe_2 and WS_2, smooth microspheres initially formed and then the nanosheets were developed and crystallized on the surface of microspheres under the solvothermal conditions. Duphil *et al.* reported an ambient solution method to produce merely amorphous WSe_2 and WS_2 irregular nanoparticles using $W(CO)_6$, Se and S in *p*-xylene.[13] Pol *et al.* previously reported a high-temperature solid reaction between $W(CO)_6$ and Se to prepare WSe_2 nanoparticles.[14] They both proposed a two-step reaction mechanism involving first the complete decomposition of $W(CO)_6$ into W and subsequent reaction of W with Se/S without giving direct evidence. In the absence of Se or S, $W(CO)_6$ was heated at varying temperatures in *p*-xylene in a Teflon-lined autoclave. The resultant products

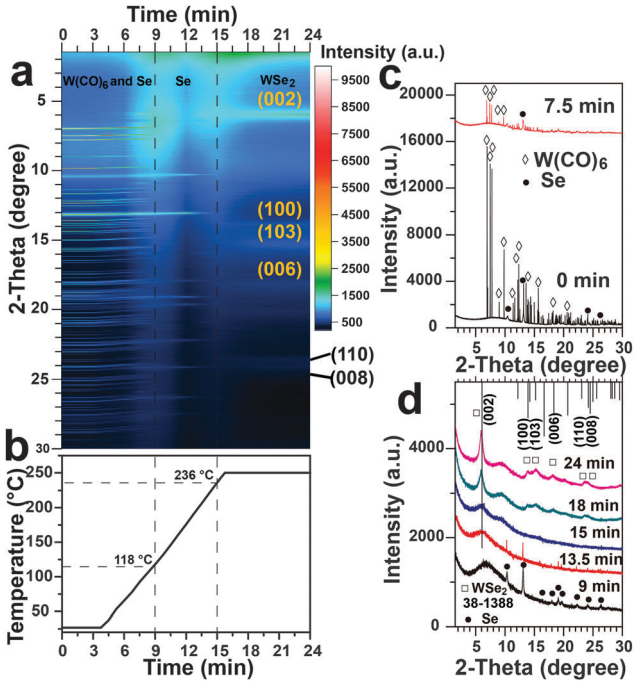

Fig. 3 (a) Time-resolved *in situ* SR-XRD patterns showing evolution from $W(CO)_6$ and Se precursors to WSe_2, (b) temperature ramp rate (20 °C min^{-1}), (c and d) characteristic SR-XRD patterns of *in situ* products at the noted reaction time. Note that the reaction rate in the micro-reactor is much faster than that of the bulk solvothermal reaction in the autoclave.

remained in the phase of $W(CO)_6$ (Fig. S10, ESI†), with no evidence of a W intermediate.

To track the phase evolution as a function of reaction time, time-resolved *in situ* SR-XRD experiments were performed. The *in situ* SR-XRD is able to provide valuable real-time phase evolution during the reaction,[1e,15] as illustrated in Scheme S1, ESI.† The *in situ* SR-XRD patterns of WSe_2 (Fig. 3) demonstrate that the solvothermal process involves dissolution of $W(CO)_6$, melting of Se and growth of flowerlike WSe_2. The *in situ* SR-XRD patterns (Fig. 2a) of the starting precursors are readily indexed to the orthorhombic phase of $W(CO)_6$ (JCPDS Card No. 40-0752) and hexagonal Se (JCPDS Card No. 06-0362), consistent with *ex situ* XRD patterns (Fig. S6, ESI†).

Upon heating in *p*-xylene, the peaks of $W(CO)_6$ continuously decreased in intensity and vanished after about 9 min at 118 °C (Fig. 3b–d). This temperature was much lower than the decomposition/melting point of $W(CO)_6$ (~170 °C) indicating that $W(CO)_6$ was neither melted nor completely decomposed into elemental tungsten. $W(CO)_6$ was likely dissolved in *p*-xylene. The peaks of the Se precursor remained until the temperature reached 236 °C (above the melting point of Se, 221 °C), when the Se precursor peak disappeared instantly. WSe_2 formed rapidly after the melting of Se. The elemental W intermediate arising from the decomposition of $W(CO)_6$ proposed in the early literature was not detected.[13,14] The formation mechanism determined from the *in situ* SR-XRD result agrees with the aforementioned *ex situ* SEM and XRD characterization. The heating rate governs the rate of Se melting and hence the whole reaction rate. Therefore, the reaction temperature plays a critical role in the formation of WSe_2. Since evidence for the formation of W was not found in either *ex situ* or *in situ* experiments, we do not deem that the reaction between dissolved $W(CO)_6$ and melted Se in *p*-xylene in this case followed the two-step process as proposed in the literature.[13,14] The reaction mechanism might be a straightforward one-step reaction, or a modified two-step process initially involving the partial dissociation of $W(CO)_6$ into $W(CO)_{6-x}$,[16] and the subsequent oxidation by Se/S atoms. The underlying mechanism will be investigated in the future through advanced *in situ* techniques (*e.g.* mass spectrometry). Besides, agglomerate WSe_2 with poor crystallinity (Fig. S11, ESI†) was obtained when $W(CO)_6$ reacted with Se without *p*-xylene, highlighting the importance of the *p*-xylene solvent in inducing the formation of flowerlike structures.

The growth process of WS_2 was also explored by the *in situ* SR-XRD (Fig. S12, ESI†). Sulfur (m.p. 115 °C) and $W(CO)_6$ were dissolved at 83 °C and 116 °C, respectively. Then WS_2 was gradually formed and crystallized upon heating. Both precursors vanished below their melting or decomposition point and no W intermediate was detected, consistent with the results of WSe_2.

The synthesis of WTe_2 at 250 °C with the solvothermal method using $W(CO)_6$ and Te (m.p. 450 °C) was attempted. However, the product was only a mixture of Te and TeO_2 with $W(CO)_6$, which was removed by rinsing with acetone (Fig. S13, ESI†).

Based on the above *ex situ* and *in situ* experimental results, the growth of WS_2 and WSe_2 began with the dissolution of S and $W(CO)_6$, melting of Se and then both precursors reacted quickly to produce crystalline WS_2 and WSe_2 under the solvothermal condition. The absence of complete dissociation of $W(CO)_6$ into W in this work appears to defy the commonly accepted two-step reaction mechanism.[13,14] The knowledge gained about the growth mechanism of tungsten sulfide and selenide by the time-resolved *in situ* SR-XRD technique will inspire new studies of various layered transition metal dichalcogenides.

These as-synthesized flowerlike WSe_2 and WS_2 microspheres possess many nanosheets and abundant chalcogen ligands with innate reactivity towards soft heavy metal ions (Hg^{2+}, Pb^{2+}, *etc.*) and structural rigidity. These features are desirable for the sequestration of heavy metal ions from water. The flowerlike WSe_2 and WS_2 microspheres were used to sequester various heavy metal ions, including As(v), As(iii), Cd^{2+}, Pb^{2+} and Hg^{2+}, from water. They did not remove As(v), As(iii) and Cd^{2+}, whereas they exhibited high uptake capacities for Hg^{2+} and Pb^{2+}. This is due to the innate selectivity of metal chalcogenides for soft heavy metal ions (*i.e.* Hg^{2+} and Pb^{2+}).[11] Fig. 4 exhibits the variation in Pb^{2+} and

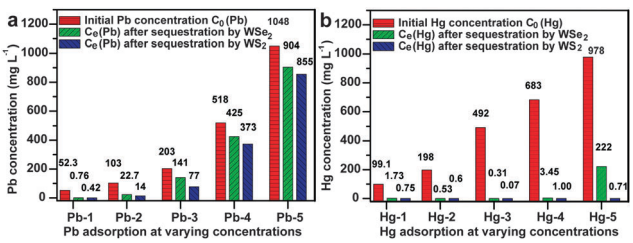

Fig. 4 (a) Pb^{2+} and (b) Hg^{2+} sequestration of WSe_2 and WS_2 in water. The WSe_2 and WS_2 content in the Pb^{2+} and Hg^{2+} aqueous solutions was 0.5 g L^{-1}.

Hg^{2+} concentrations before and after sequestration by WSe_2 and WS_2 samples at 0.5 g L^{-1}. The WSe_2 and WS_2 were able to reduce the concentration of Pb^{2+} from 52.30 mg L^{-1} to 0.76 and 0.42 mg L^{-1} (Fig. 4a), respectively, giving a Pb^{2+} uptake capacity of *ca.* 103 mg g^{-1}. The highest Pb^{2+} uptake capacities of WSe_2 and WS_2 are 288 and 386 mg g^{-1} when treating 1048 mg L^{-1} of lead ions in water, which are substantially higher than those of nanostructured adsorbents with abundant hydroxyl groups reported previously, such as urchin-like FeOOH (80 mg g^{-1}),[8a] flowerlike zinc silicate (210 mg g^{-1}) and flowerlike AlOOH (124.2 mg g^{-1}) under similar conditions (Table S1, ESI†).[8c,10] Particularly, WSe_2 and WS_2 show extremely high uptake capacities for Hg^{2+} (Fig. 4b). WSe_2 and WS_2 could decrease the concentration of Hg^{2+} from 978 mg L^{-1} to 222 mg L^{-1} and 0.71 mg L^{-1} resulting in impressive capacities of 1512 mg g^{-1} and 1954 mg g^{-1}, respectively. Their capacities for Hg^{2+} are significantly higher than those of conventional metal oxide and carbon-based adsorbents (Table S1, ESI†) and those of metal chalcogenides (Table S2, ESI†).[11] Flowerlike WSe_2 was characterized after removal of Pb^{2+} and Hg^{2+} (Fig. S14 & S15, ESI†). $PbWO_4$ polyhedron nanoparticles are embedded in the WSe_2 nanosheets suggesting that Pb^{2+} ions were removed *via* a chemical reaction. When treating Hg^{2+} ions in water, the WSe_2 nanosheets were almost fully covered by Hg_2Cl_2 and $Hg_3Se_2Cl_2$ nanoparticles, suggesting that WSe_2 is a reducing agent that has high reactivity towards Hg^{2+} leading to the high Hg^{2+} uptake capacity. Likewise, $PbWO_4$ nanoparticles are immobilized on WS_2 nanosheets (Fig. S16 & S17, ESI†). WS_2 microspheres are enclosed by as-formed $Hg_3S_2Cl_2$ and Hg_2Cl_2 particles, indicating extremely high reactivity and reducibility of WS_2 towards Hg^{2+} ions, which resulted in such a high Hg^{2+} sequestration capacity. The WS_2 microsphere is superior to the flowerlike WSe_2 in terms of uptake capacities for Pb^{2+} and Hg^{2+}, possibly because sulfide has higher reactivity towards Pb^{2+} and Hg^{2+} than selenide. This mechanism is different from the direct cation exchange mechanism of other metal chalcogenides for heavy metal ion sequestration.[11]

In summary, flowerlike WSe_2 and WS_2 microspheres assembled of nanosheets were synthesized by a facile and high-yield solvothermal method. The *in situ* SR-XRD gave insights into the growth mechanism of the flowerlike WSe_2 and WS_2, which is the reaction between dissolved $W(CO)_6$ and dissolved S or melted Se without complete decomposition of $W(CO)_6$ into a W intermediate. Flowerlike WSe_2 and WS_2 microspheres were used for heavy metal ion sequestration and exhibited remarkable uptake capacities for Pb^{2+} (288 mg g^{-1} for WSe_2 and 386 mg g^{-1} for WS_2) and Hg^{2+} (1512 mg g^{-1} for WSe_2 and 1954 mg g^{-1} for WS_2), showing great potential in heavy metal remediation. The synthesis method and SR-XRD characterization in this work offer novel approaches towards rational design and fabrication of hierarchical transition metal dichalcogenides and understanding of their formation mechanism.

This project received financial support from Joint Research Project funding (GJHZ1224) from the Chinese Academy of Sciences and CSIRO. We acknowledge the Australian Synchrotron for the Powder Diffraction beamline access, and CSIRO Minerals for laboratory *in situ* XRD access. The CSIRO Office of the Chief Executive (OCE) Postdoctoral and Science Leader Schemes are acknowledged for supporting this work. R. A. C. acknowledges the Australian Research Council for a Future Fellowship (FT0990583).

Notes and references

1 (*a*) Q. H. Wang, K. Kalantar-Zadeh, A. Kis, J. N. Coleman and M. S. Strano, *Nat. Nanotechnol.*, 2012, **7**, 699–712; (*b*) X. Huang, Z. Y. Zeng and H. Zhang, *Chem. Soc. Rev.*, 2013, **42**, 1934–1946; (*c*) R. Lv, J. A. Robinson, R. E. Schaak, D. Sun, Y. Sun, T. E. Mallouk and M. Terrones, *Acc. Chem. Res.*, 2015, **48**, 56–64; (*d*) M. R. Gao, Y. F. Xu, J. Jiang and S. H. Yu, *Chem. Soc. Rev.*, 2013, **42**, 2986–3017; (*e*) J. Song, F. Xia, M. Zhao, Y. L. Zhong, W. Li, K. P. Loh, R. A. Caruso and Q. Bao, *Chem. Mater.*, 2015, **27**, 3471–3482; (*f*) X. Liu, J. Xu, Z. Fang, L. Lin, Y. Qian, Y. Wang, C. Ye, C. Ma and J. Zeng, *Nano Res.*, 2015, **8**, 3612–3620.

2 J. Kim, X. P. Hong, C. H. Jin, S. F. Shi, C. Y. S. Chang, M. H. Chiu, L. J. Li and F. Wang, *Science*, 2014, **346**, 1205–1208.

3 (*a*) B. Liu, T. Luo, G. Y. Mu, X. F. Wang, D. Chen and G. Z. Shen, *ACS Nano*, 2013, **7**, 8051–8058; (*b*) D. Chen, G. Ji, B. Ding, Y. Ma, B. Qu, W. Chen and J. Y. Lee, *Nanoscale*, 2013, **5**, 7890–7896.

4 (*a*) H. T. Wang, D. S. Kong, P. Johanes, J. J. Cha, G. Y. Zheng, K. Yan, N. A. Liu and Y. Cui, *Nano Lett.*, 2013, **13**, 3426–3433; (*b*) K. Xu, F. M. Wang, Z. X. Wang, X. Y. Zhan, Q. S. Wang, Z. Z. Cheng, M. Safdar and J. He, *ACS Nano*, 2014, **8**, 8468–8476; (*c*) L. Cheng, W. J. Huang, Q. F. Gong, C. H. Liu, Z. Liu, Y. G. Li and H. J. Dai, *Angew. Chem., Int. Ed.*, 2014, **53**, 7860–7863.

5 (*a*) J. R. McKone, A. P. Pieterick, H. B. Gray and N. S. Lewis, *J. Am. Chem. Soc.*, 2013, **135**, 223–231; (*b*) Y. H. Sang, Z. H. Zhao, M. W. Zhao, P. Hao, Y. H. Leng and H. Liu, *Adv. Mater.*, 2015, **27**, 363–369.

6 L. X. Lin, Y. X. Xu, S. W. Zhang, I. M. Ross, A. C. M. Ong and D. A. Allwood, *ACS Nano*, 2013, **7**, 8214–8223.

7 (*a*) T. Georgiou, R. Jalil, B. D. Belle, L. Britnell, R. V. Gorbachev, S. V. Morozov, Y. J. Kim, A. Gholinia, S. J. Haigh, O. Makarovsky, L. Eaves, L. A. Ponomarenko, A. K. Geim, K. S. Novoselov and A. Mishchenko, *Nat. Nanotechnol.*, 2013, **8**, 100–103; (*b*) H. Fang, S. Chuang, T. C. Chang, K. Takei, T. Takahashi and A. Javey, *Nano Lett.*, 2012, **12**, 3788–3792.

8 (*a*) B. Wang, H. Wu, L. Yu, R. Xu, T.-T. Lim and X. W. Lou, *Adv. Mater.*, 2012, **24**, 1111–1116; (*b*) H. Li, W. Li, Y. Zhang, T. Wang, B. Wang, W. Xu, L. Jiang, W. Song, C. Shu and C. Wang, *J. Mater. Chem.*, 2011, **21**, 7878–7881; (*c*) Y.-X. Zhang, Y. Jia, Z. Jin, X.-Y. Yu, W.-H. Xu, T. Luo, B.-J. Zhu, J.-H. Liu and X.-J. Huang, *CrystEngComm*, 2012, **14**, 3005–3007; (*d*) S. Hu, W. Chen, J. Zhou, F. Yin, E. Uchaker, Q. Zhang and G. Cao, *J. Mater. Chem. A*, 2014, **2**, 7862–7872; (*e*) W. Li, D. H. Chen, F. Xia, J. Z. Y. Tan, P.-P. Huang, W.-G. Song, N. M. Nursam and R. A. Caruso, *Environ. Sci.: Nano*, 2016, **3**, 94–106; (*f*) X. Li, W. Li, M. Li, P. Cui, D. H. Chen, T. Gengenbach, L. Chu, H. Liu and G. Song, *J. Mater. Chem. A*, 2015, **3**, 2762–2769; (*g*) C. Chen, Y. Yu, W. Li, C. Cao, P. Li, Z. Dou and W.-G. Song, *J. Mater. Chem.*, 2011, **21**, 12836–12841.

9 (*a*) A. Prabakaran, F. Dillon, J. Melbourne, L. Jones, R. J. Nicholls, P. Holdway, J. Britton, A. A. Koos, A. Crossley, P. D. Nellist and N. Grobert, *Chem. Commun.*, 2014, **50**, 12360–12362; (*b*) Z. L. Yang, D. Q. Gao, J. Zhang, Q. Xu, S. P. Shi, K. Tao and D. S. Xue, *Nanoscale*, 2015, **7**, 650–658.

10 J. Qu, C.-Y. Cao, Y.-L. Hong, C.-Q. Chen, P.-P. Zhu, W.-G. Song and Z.-Y. Wu, *J. Mater. Chem.*, 2012, **22**, 3562–3567.

11 (*a*) I. R. Pala and S. L. Brock, *ACS Appl. Mater. Interfaces*, 2012, **4**, 2160–2167; (*b*) M. J. Manos, C. D. Malliakas and M. G. Kanatzidis, *Chem. – Eur. J.*, 2007, **13**, 51–58; (*c*) M. J. Manos, V. G. Petkov and M. G. Kanatzidis, *Adv. Funct. Mater.*, 2009, **19**, 1087–1092; (*d*) C. W. Abney, J. C. Gilhula, K. Lu and W. Lin, *Adv. Mater.*, 2014, **26**, 7993–7997; (*e*) M. J. Manos and M. G. Kanatzidis, *Chem. – Eur. J.*, 2009, **15**, 4779–4784.

12 N. D. Boscher, C. J. Carmalt and I. P. Parkin, *J. Mater. Chem.*, 2006, **16**, 122–127.

13 D. Duphil, S. Bastide, J. C. Rouchaud, J. L. Pastol, B. Legendrel and C. Levy-Clement, *Nanotechnology*, 2004, **15**, 828–832.

14 S. V. Pol, V. G. Pol, J. M. Calderon-Moreno and A. Gedanken, *J. Phys. Chem. C*, 2008, **112**, 5356–5360.

15 W. Li, F. Xia, J. Qu, P. Li, D. H. Chen, Z. Chen, Y. Yu, Y. Lu, R. A. Caruso and W.-G. Song, *Nano Res.*, 2014, **7**, 903–916.

16 N. Wiberg and A. F. Holleman, *Inorganic Chemistry*, 2001, Academic Press.